Commun. Comput. Phys.
doi: 10.4208/cicp.220715.150416a

Vol. **21**, No. 2, pp. 570-599
February 2017

# An Implicitly Consistent Formulation of a Dual-Mesh Hybrid LES/RANS Method

Heng Xiao[1,*], Jian-Xun Wang[1] and Patrick Jenny[2]

[1] *Department of Aerospace and Ocean Engineering, Virginia Tech, Blacksburg, VA 24060, USA.*
[2] *Institute of Fluid Dynamics, ETH Zürich, 8092 Zurich, Switzerland.*

Received 22 July 2015; Accepted (in revised version) 15 April 2016

**Abstract.** A consistent dual-mesh hybrid LES/RANS framework for turbulence modeling has been proposed recently (H. Xiao, P. Jenny, A consistent dual-mesh framework for hybrid LES/RANS modeling, J. Comput. Phys. 231 (4) (2012)). To better enforce componentwise Reynolds stress consistency between the LES and the RANS simulations, in the present work the original hybrid framework is modified to better exploit the advantage of more advanced RANS turbulence models. In the new formulation, the turbulent stresses in the filtered equations in the under-resolved regions are directly corrected based on the Reynolds stresses provided by the RANS simulation. More precisely, the new strategy leads to implicit LES/RANS consistency, where the velocity consistency is achieved indirectly via imposing consistency on the Reynolds stresses. This is in contrast to the explicit consistency enforcement in the original formulation, where forcing terms are added to the filtered momentum equations to achieve directly the desired average velocity and velocity fluctuations. The new formulation keeps the averaging procedure for the filtered quantities and at the same time preserves the ability of the original formulation to conform with the physical differences between LES and RANS quantities. The modified formulation is presented, analyzed, and then evaluated for plane channel flow and flow over periodic hills. Improved predictions are obtained compared with the results obtained using the original formulation.

**AMS subject classifications**: 76F65

**Key words**: Hybrid LES/RANS methods, turbulence modeling, wall-bounded flow.

## 1 Introduction

In the past two decades Large Eddy Simulation (LES) has been successfully used to study flows in a wide variety of applications. However, its high computational cost for wall-

*Corresponding author. *Email addresses:* hengxiao@vt.edu (H. Xiao), vtwjx@vt.edu (J.-X. Wang), jenny@ifd.mavt.ethz.ch (P. Jenny)

 ©2017 Global-Science Press

https://doi.org/10.4208/cicp.220715.150416a Published online by Cambridge University Press

bounded flows at high Reynolds numbers still is a major hurdle for applications to practical flows in industry and nature [1]. This is due to the difficulty in resolving the small but important near-wall eddies in LES, since the computational cost of resolving such eddies scales as $Re^{1.8}$ according to Chapman [2] or $Re^{13/7}$ according to a more recent estimation by Choi and Moin [3], where $Re$ is the Reynolds number. To overcome this difficulty, many hybrid LES/RANS (Reynolds Averaged Navier-Stokes) methods have been proposed, where the RANS equations are solved in the near-wall region and LES is conducted in the free-shear domain away from walls. In this strategy statistics of the small eddies near the wall is computed by a RANS model instead of being resolved in an LES.

Recently, Xiao and Jenny [4] developed a novel hybrid LES/RANS framework, where LES and RANS simulations are conducted simultaneously on the entire domain on separate meshes. Relaxation forces are applied on the respective equations to ensure consistency between the two solutions, hence the designation *consistent dual-mesh* hybrid LES/RANS framework. Within this framework, a hybrid LES/RANS solver for incompressible flows called HybridLRFoam has been developed based on the open-source CFD platform OpenFOAM [5]. Preliminary investigations were conducted of plane channel flow and of flow over periodic hills at different Reynolds numbers. The results show that the proposed method leads to satisfactory results on relatively coarse meshes, which is promising for industrial flow simulations [4, 6]. Xiao et al. [7] extended the original solver by utilizing a high-order, Cartesian-mesh-based in-house LES solver IMPACT [8,9] in lieu of the second-order OpenFOAM-based LES solver in HybridLRFoam. A volume-penalization method was used to impose wall boundary conditions for IMPACT. The two hybrid solvers differ only in the LES solver used and are based on the same coupling scheme. The obtained solver, named ImpactFoam, demonstrated the flexibility of the coupling scheme in accommodating different RANS and LES solvers.

In both HybridLRFoam [4, 6] and ImpactFoam [7] the relatively simple two-equation $k$–$\varepsilon$ model of Launder and Sharma [10] was used, although the proposed framework is flexible enough to accommodate other RANS turbulence models. For the periodic hill test case, the solver led to excellent predictions in the attached regions for both mean velocity profiles and wall friction coefficients. However, in the separated region the prediction of the hybrid solver was not completely satisfactory. A likely reason therefore is the limitations of the relatively simple RANS model which was active in this region. It is well-known that $k$–$\varepsilon$ models do not perform well in flows with recirculation and adverse pressure gradients. Billard [11] evaluated several eddy-viscosity models and Reynolds stress transport models for flow over periodic hills and other separating flows. Among the models he evaluated the Reynolds stress transport model with elliptic relaxation led to the best prediction of flow separations, and they emphasized that careful selection of the underlying RANS model in a hybrid LES/RANS approach is very important.

A Reynolds Stress Transport Model with Elliptic Relaxation (RSTM-ER) was proposed by Durbin [12] based on the LRR Reynolds stress transport model of Rodi et al. [13]. In this model, an elliptic operator takes into account the non-local effects of the wall on

https://doi.org/10.4208/cicp.220715.150416a Published online by Cambridge University Press

the pressure-rate-of-strain tensor, a feature that distinguishes such closures from other wall-resolving models based on ad hoc damping functions. The near-wall regions have to be adequately resolved in wall-normal direction. Due to its physically sophisticated non-localness, the RSTM-ER is better suited for separating flows than local models or models based on wall functions. In conclusion, it can be stated that the RSTM-ER is a very suitable candidate for closure of the RANS part in the consistent hybrid LES/RANS framework; for the work presented here the RSTM-ER of Durbin [12] was implemented. While several other variants of the RSTM-ER have been proposed based on Durbin's formulation [14–17], in this work we limit the attention to the original formulation of Durbin, although theoretically the modified RSTM-ER formulations may perform better and/or may be computationally cheaper. Note, however, that it was not the aim of this work to compare the performance of different variants and formulations of RSTM.

While choosing a proper RANS turbulence model is certainly critical for the performance of the hybrid solver, obtaining accurate RANS predictions in the near-wall region completes only part of the mission. The ultimate objective of the hybrid framework is to achieve good LES predictions by including information provided by the RANS solver in the near-wall region. Effectively taking advantage of the near-wall predictions from the RANS solution to improve the LES solution is a major challenge. Numerous mathematical approaches have been developed to combine the advantages of RANS and LES, including Detached Eddy Simulation (DES) [18], Partially Averaged Navier-Stokes equations (PANS) [19], Partially Integrated Transport Model (PITM) [20, 21], multiple scale models [22, 23], Very Large Eddy Simulation (VLES) [24], among others. A noteworthy recent development is the Reynolds Stress Constrained Large Eddy Simulation (RSC-LES) developed by S. Chen and his co-workers at Peking University [25, 26], which will be detailed below.

The most straightforward idea to combine RANS and LES in the same framework is to replace the modeled residual stresses in the near-wall region with the Reynolds stresses provided by RANS solutions. This is the strategy used in most existing models including DES. However, this strategy leads to inconsistencies between filtered and Reynolds-averaged quantities at the LES/RANS interfaces or in the transition regions. Specifically, Reynolds-averaged velocities are solved for in RANS simulations while filtered velocities are solved for in LES, and despite the different physical meaning of the two quantities, at the interface or the transition regions they are treated in the same way, and thus the interpretation of the obtained results are not clear. On the RANS simulation side the Reynolds averaged stresses lead to strong damping of the velocity fluctuations, which leads to unphysically strong damping of the filtered velocity fluctuations on the LES side. This so-called modeled stress depletion (MSD) leads to log-layer mismatch in the mean velocity profiles [27, 28]. This issue has been widely recognized in the hybrid LES/RANS community. In the RSC-LES method mentioned above, the entire domain is solved with LES, which avoids any LES-to-RANS transition region that is the root cause of the log-layer mismatch. In the near-wall region where the LES is under-resolved, a Reynolds stress constraint is enforced on the SGS model of the LES to ensure that the sta-

https://doi.org/10.4208/cicp.220715.150416a Published online by Cambridge University Press

tistical moments of the instantaneous Reynolds stress is consistent with those obtained from the RANS. Away from the wall where the LES adequately resolves the flow, the constraint is removed. Evaluations and applications on practical flows (e.g., flow past airfoil [29], flow in a channel with periodic hills [30], flow in a U-duct [31]) have shown promising results.

A somewhat similar strategy was adopted in the consistent hybrid framework of Xiao and Jenny [4], where both LES and RANS equations are solved on the whole domain. In the near-wall, under-resolved region, the filtered velocities are enhanced or damped to achieve consistency with the RANS solution. Although theoretically this is an elegant approach, the numerical implementation requires care, mainly since only three velocity components can be directly altered to achieve agreement for the six independent Reynolds stresses. Moreover, another potential problem of the original framework is the potential loss of momentum conservation, i.e., the forcing terms are not divergence-free and may act as momentum sink or source in the interior of the flow; this may not be an issue for periodic flows where the flows were driven by pressure gradient to achieve specified bulk flow velocity, but may be a significant issue for general flows.

In this work, to combine the consistency feature of the original formulation of the hybrid LES/RANS framework [4] and the forcing strategy used by other hybrid methods, we propose a formulation with a modified forcing strategy. In this modified formulation the turbulent stresses are directly corrected, which allows for a direct use of the RANS Reynolds stress in the LES. On the other hand, the averaging procedure in the original formulation is preserved, which is essential to reflect the physical differences between LES and RANS quantities, and to avoid LES/RANS inconsistencies and modeled stress depletion.

The rest of this paper is organized as follows. In Section 2, the original formulation of the consistent hybrid LES/RANS framework [4] is summarized, and the modified formulation is presented. The implementation of the hybrid solver, the numerical methods, and the turbulence models are introduced in Section 3. Numerical simulations based on the modified formulation are presented in Section 4 with comparison to the results from the original formulation. The advantages and drawbacks of the consistent hybrid framework are discussed in Section 5, and finally the paper is concluded in Section 6.

## 2 Dual-mesh hybrid LES/RANS framework: Formulations

### 2.1 Hybrid LES/RANS framework with explicit consistency

For simplicity, we consider incompressible flows with constant density. The momentum and pressure equations for the filtered and the Reynolds-averaged quantities can be writ-

https://doi.org/10.4208/cicp.220715.150416a Published online by Cambridge University Press

ten in a unified form as follows [4]:

$$\frac{\partial U_i^*}{\partial t}+\frac{\partial\left(U_i^*U_j^*\right)}{\partial x_j}=-\frac{1}{\rho}\frac{\partial p^*}{\partial x_i}+\nu\frac{\partial^2 U_i^*}{\partial x_j\partial x_j}-\frac{\partial\tau_{ij}^*}{\partial x_j}+Q_i^*, \tag{2.1a}$$

$$\frac{1}{\rho}\frac{\partial^2 p^*}{\partial x_i\partial x_i}=-\frac{\partial^2}{\partial x_i\partial x_j}\left(U_i^*U_j^*+\tau_{ij}^*\right)+\frac{\partial Q_i^*}{\partial x_i}, \tag{2.1b}$$

where $t$ and $x_i$ are time and space coordinates, respectively; $\nu$ is the kinematic viscosity, $\rho$ is the constant fluid density, and $p^*$ is the pressure. In the filtered equations, $U_i^*$, $p^*$, and $\tau_{ij}^*$ represent filtered velocity $\overline{U}_i$, filtered pressure $\overline{p}$, and residual stresses $\tau_{ij}^{\rm sgs}$, respectively. In Reynolds-averaged equations, $U_i^*$, $p^*$, and $\tau_{ij}^*$ represent Reynolds-averaged velocity $\langle U_i\rangle^{\rm RANS}$, Reynolds-averaged pressure $\langle p\rangle^{\rm RANS}$, and Reynolds stresses $\tau_{ij}$, respectively. The Reynolds stress $\tau_{ij}=\langle u_i'u_j'\rangle^{\rm RANS}$ is defined as the correlation of velocity fluctuations, although the apparent Reynolds stresses are actually $-\langle u_i'u_j'\rangle^{\rm RANS}$. The source term $Q_i^*$ represents the drift forces applied in the filtered equations ($Q_i^L$) and in the Reynolds-averaged equations ($Q_i^R$) to ensure consistency between the two solutions. This term will be detailed in Eqs. (2.7) and (2.8).

In this hybrid framework, the filtered equations and the Reynolds-averaged equations are solved simultaneously in the entire domain but on separate meshes. This leads to some redundancy, and the consistency is enforced with $Q_i^*$.

Recognizing the fact that the filtered quantities in LES and the Reynolds-averaged quantities in the RANS equations have different physical interpretations, we first introduce Exponentially Weighted Average (EWA, or simply referred to as *average* hereafter, if the meaning is clear from the context) operation for any quantity $\phi$ as

$$\langle\phi\rangle^{\rm AVG}(t)=\frac{1}{T}\int_{-\infty}^{t}\phi(t')e^{-(t-t')/T}dt', \tag{2.2}$$

then the EWA velocity, dissipation, and turbulent stress for the LES can be simplified to the following after a number of assumptions discussed later:

$$\langle\overline{U}_i\rangle^{\rm AVG}(t)=\frac{1}{T}\int_{-\infty}^{t}\overline{U}_i(t')e^{-(t-t')/T}dt', \tag{2.3a}$$

$$\langle\tau_{ij}\rangle^{\rm AVG}(t)=\frac{1}{T}\int_{-\infty}^{t}\left[u_i''(t')u_j''(t')+\tau_{ij}^{\rm sgs}(t')\right]e^{-(t-t')/T}dt', \quad \text{and} \tag{2.3b}$$

$$\langle\varepsilon\rangle^{\rm AVG}(t)=\frac{1}{T}\int_{-\infty}^{t}\left[2\nu\overline{S}_{ij}(t')\overline{S}_{ij}(t')-\tau_{ij}^{\rm sgs}(t')\overline{S}_{ij}(t')-2\nu\langle\overline{S}_{ij}\rangle^{\rm AVG}\langle\overline{S}_{ij}\rangle^{\rm AVG}\right]e^{-(t-t')/T}dt', \tag{2.3c}$$

respectively, where $T$ is the averaging time scale and

$$u_i''=\overline{U}_i-\langle\overline{U}_i\rangle^{\rm AVG} \tag{2.4}$$

https://doi.org/10.4208/cicp.220715.150416a Published online by Cambridge University Press

is the fluctuating velocity with respect to the exponentially weighted average. The terms inside the integral of Eq. (2.3b) are the total turbulent stress in the LES, denoted as

$$\tau_{ij}^{\mathrm{LES}} = u_i'' u_j'' + \tau_{ij}^{\mathrm{sgs}}, \tag{2.5}$$

where $u_i'' u_j''$ is the resolved part and $\tau_{ij}^{\mathrm{sgs}}$ is the modeled part. Similarly, the terms in the integrand in Eq. (2.3c) represents the total dissipation rate in LES including the resolved and modeled parts. The rate-of-strain tensor based on the filtered velocities is

$$\overline{S}_{ij} = \frac{1}{2}\left(\frac{\partial \overline{U}_i}{\partial x_j} + \frac{\partial \overline{U}_j}{\partial x_i}\right). \tag{2.6}$$

To achieve consistency between the two solutions, it is required that the exponentially weighted average quantities and the Reynolds-averaged quantities are approximately equal, e.g., $\langle \overline{U}_i \rangle^{\mathrm{AVG}} \approx \langle U_i \rangle^{\mathrm{RANS}}$ for the velocities and $\langle \tau_{ij} \rangle^{\mathrm{AVG}} \approx \tau_{ij}$ for the turbulent stresses. The regions which are well-resolved by the LES mesh are classified as LES regions where the LES solution should dominate, and the under-resolved regions are called RANS regions where the RANS solution shall be dominant. Consistency in these selected subdomains is enforced via the drift terms $Q_i^L$ (in the filtered equations) and $Q_i^R$ (in the Reynolds-averaged equations); they are defined as follows:

$$Q_i^L = \begin{cases} \underbrace{\left(\langle U_i \rangle^{\mathrm{RANS}} - \langle \overline{U}_i \rangle^{\mathrm{AVG}}\right)/T^{(\mathrm{L})}}_{Q_i^{(\mathrm{LU})}} + \underbrace{G_{ij} u_j'' / T^{(\mathrm{G})}}_{Q_i^{(\mathrm{LG})}} & \text{in RANS regions;} \\ 0 & \text{in LES regions} \end{cases} \tag{2.7}$$

and

$$Q_i^R = \begin{cases} 0 & \text{in RANS regions;} \\ \left(\langle \overline{U}_i \rangle^{\mathrm{AVG}} - \langle U_i \rangle^{\mathrm{RANS}}\right)/T^{(\mathrm{R})} & \text{in LES regions,} \end{cases} \tag{2.8}$$

where

$$G_{ij} = \frac{\tau_{ij} - \langle \tau_{ij} \rangle^{\mathrm{AVG}}}{\langle \tau_{kk} \rangle^{\mathrm{AVG}}}, \tag{2.9}$$

with the relaxation time scales $T^{(\mathrm{L})}$, $T^{(\mathrm{G})}$, and $T^{(\mathrm{R})}$. Subscripts $i$, $j$, and $k$ are used as indices.

Similarly, to ensure consistency on the turbulent quantities in the RANS simulation, in the well-resolved (LES) regions they are relaxed towards the corresponding LES quantities via the added drift terms. Detailed solution algorithm and the choice of parameters are presented in Xiao and Jenny [4].

## 2.2 Hybrid LES/RANS framework with implicit consistency

The forcing $Q_i^L$ applied on the filtered equations in the under-resolved regions consists of two terms, as can be seen from Eq. (2.7). The first term enforces consistency of mean

https://doi.org/10.4208/cicp.220715.150416a Published online by Cambridge University Press

velocities, i.e., consistency between the first moment of the filtered instantaneous velocity and the Reynolds-averaged velocity. This is relatively easy to achieve, which has been demonstrated previously [4]. The second term enforces turbulent stress consistency, i.e., the consistency between the second moments of filtered velocity and the Reynolds stresses in the RANS, which is achieved by scaling the velocity fluctuations. The turbulent stress tensor has six independent components, representing the correlations among the three velocity components. Our experience suggests that achieving componentwise turbulent stress consistency, particularly for the cross-correlations (i.e., for the turbulent shear stresses), is very challenging in practical simulations. This is because (1) forcing is applied on three degrees of freedom, but consistency is required for six independent components of the Reynolds stresses; and (2) the time scales (or frequencies) of the drift forcing terms to achieve Reynolds stress consistency may be of the same order as those of the other internal forces in the flow system described by the Navier-Stokes equations.

Xiao and Jenny [4] only enforced consistency on the turbulent kinetic energy (i.e., the trace of the turbulent stress tensor). This is partly because an eddy viscosity turbulence model was used in the RANS solver, which does not provide reliable Reynolds stress predictions, particularly near the wall. Note that this is an intrinsic deficiency of all models based on Boussinesq assumption. Therefore, this framework has potential that can be explored by requiring better turbulent stress consistency.

To this end, we propose the strategy of enforcing the consistency by modifying the mean turbulent stress, and not by scaling the fluctuations as in the original formulation. This is achieved by correcting the Reynolds stress according to the consistency requirement and formulating the relaxation forces accordingly, i.e., by using the following expression for $Q_i^L$ in lieu of Eq. (2.7):

$$Q_i^L = \begin{cases} -\frac{\partial}{\partial x_j}(\tau_{ij}^{\text{corr}}) & \text{in RANS regions;} \\ 0 & \text{in LES regions,} \end{cases} \tag{2.10}$$

with

$$\tau_{ij}^{\text{corr}} = \tau_{ij} - \left( \langle u_i'' u_j'' \rangle^{\text{AVG}} + \langle \tau_{ij}^{\text{sgs}} \rangle^{\text{AVG}} \right), \tag{2.11}$$

where $\langle u_i'' u_j'' \rangle^{\text{AVG}}$ and $\langle \tau_{ij}^{\text{sgs}} \rangle^{\text{AVG}}$ are resolved and averaged modeled turbulent stresses in LES, respectively.

In additional to the heuristic motivation above, a more formal (albeit still not rigorous) justification is outlined below. The derivation is analogous to the derivation of RANS equations from the Navier-Stokes equations (e.g., Chapter 4 of Pope [32]). The following assumptions are made in this work to facilitate our derivations:

(i) the averaging operator $\langle \cdot \rangle^{\text{AVG}}$ as defined in Eqs. (2.2) and (2.3) is equivalent to the Reynolds-averaging operator $\langle \cdot \rangle^{\text{RANS}}$, i.e., for the velocity $\overline{U}_i$ or any other quantity

https://doi.org/10.4208/cicp.220715.150416a Published online by Cambridge University Press

we define $u_i''$ as in Eq. (2.4), and consequently following relations hold:

$$\langle u_i'' \rangle^{\mathrm{AVG}} = 0, \tag{2.12a}$$

$$\langle \langle \overline{U}_i \rangle^{\mathrm{AVG}} \rangle^{\mathrm{AVG}} = \langle \overline{U}_i \rangle^{\mathrm{AVG}}, \tag{2.12b}$$

$$\langle \langle \overline{U}_i \rangle^{\mathrm{AVG}} u_j'' \rangle^{\mathrm{AVG}} = \langle \overline{U}_i \rangle^{\mathrm{AVG}} \langle u_j'' \rangle^{\mathrm{AVG}} = 0; \tag{2.12c}$$

(ii) the RANS equations are close to steady state and thus the amount of resolved Reynolds stress is negligible compared with the modeled one.

These assumptions hold only for statistically stationary flows and with averaging time $T \to \infty$. For other flows in general they are only approximate and thus the procedure below is not mathematically rigorous. Moreover, in LES/RANS transition regions the averaging would be even more complicated, and the assumptions above may not be valid. This simplification is, however, in line with other assumptions in the hybrid framework. For convenience, these assumptions are referred to as *stationary turbulence assumption* below.

The detailed derivation procedure and the reasoning follow closely those presented by Chen et al. [25], but differences exist in the assumptions, the interpretations, and the implementation strategies. Specifically, Chen et al. [25] obtained the constraints on LES modeled stresses in the under-resolved region by first performing ensemble averaging on the filtered equations solved in LES and then comparing them with the RANS equations. The exponential averaging process was also used in Chen's group to simulate more complex flow problems. This procedure is what we used here as well, which is shown in the exponential averaging operator as defined in Eq. (2.3) and is justified by the assumptions above. Furthermore, a major difference is that we used separate meshes for the RANS and the LES with the RANS mesh adequately resolving the wall following our original framework. Chen et al. [25], on the other hand, used a single mesh. The RANS models we investigated in this work are advanced RSTM models that are intended to handle more challenging flows such as those with flow separations. This is in contrast to the algebraic stress model and SA model [33] explored in [25]. Finally, the emphasis of the present work is placed on the detailed investigation of different components of the hybrid method (RANS model selection, LES/RANS interface detection method, and forcing strategy) on the overall performance, which is achieved by well controlled studies. Considering both the similarity of our derivation procedure and the differences detailed above compared to those of Chen et al. [25], we presented our derivation in the Appendix for completeness.

Based on the reasoning above, the modified formulation for the forcing is based on consistency between Reynolds-averaged quantities and the averaged filtered quantities; not between Reynolds-averaged and instantaneous filter quantities. Therefore, the modified formulation preserves a fundamental feature of the original formulation, i.e., the ability of sustaining fluctuations in the LES. The new forcing is based on modifying the turbulent stresses, but unlike the forcing term in the original formulation of Eq. (2.7), consistency is only enforced implicitly. Specifically, in contrast to the relaxing forcing in the

https://doi.org/10.4208/cicp.220715.150416a Published online by Cambridge University Press

original formulation, which relaxes RANS velocities and averaged LES velocities towards each other in the respective regions, the new forcing in the modified formulation does not explicitly reduce the differences between RANS velocities and averaged LES velocities. However, it does ensure that the Reynolds stresses in the RANS solver and the averaged turbulent stresses in the LES are equal. Hence, the RANS velocities and averaged LES velocities should theoretically be consistent throughout the domain, although the consistency is not enforced explicitly on the velocities. Therefore, the modified framework is referred to as *implicitly consistent hybrid formulation*. We write the new formulation to unify it formally with the original formulation in Ref. [4], but the nature of the current formulation is fundamentally different. Specifically, although in both cases the exponentially weighted average velocities in the LES are forced, in the current formulation the forcing is achieved via correcting the average turbulent stresses, while in the original formulation the forcing is directly related to the average velocity itself (proportional to the differences between the LES averaged velocity and the RANS velocity).

To further illustrate the properties of the new formulation, we make the following observations about the Reynolds stress corrections. The correction $\tau_{ij}^{\text{corr}}$ is applied to account for the difference between the Reynolds stress $\tau_{ij}$ in RANS simulation and the *averaged* turbulent stresses $\langle\tau_{ij}^{\text{LES}}\rangle^{\text{AVG}}$ in LES (including the resolved part and the modeled part; see Eq. (2.5)). This is in contrast to the common zonal models (e.g., DES), where Reynolds stresses are usually used *in place of* the sub-grid scale (SGS) stress in LES. In the hybrid formulation of Uribe et al. [34], the turbulence stresses are computed as a blending of those obtained from SGS and RANS turbulence models: $\tau_{ij}^{\text{hybrid}}=f_b\tau_{ij}^{\text{sgs}}+(1-f_b)\tau_{ij}^{\text{RANS}}$, where the blending factor $f_b$ is a smooth function ranging from 0 to 1. The novelty of their formulation is that they used the averaged filtered velocity (corresponding to $\langle\overline{U_i}\rangle^{\text{AVG}}$ in our work) in the RANS turbulence model to compute $\tau_{ij}^{\text{RANS}}$. This is a significant improvement over DES, where instantaneous velocities are used. The blending function is an essential component of their formulation. In contrast, the transition from LES to RANS region is abrupt in the proposed model, i.e., at any time a cell is either a LES cell or a RANS cell. No blending of LES and RANS is performed explicitly. Nevertheless, in average such a blending can occur effectively when the LES/RANS interfaces are determined dynamically, i.e., when a cell is classified as LES cell during part of the simulation and as RANS cell during other time.

It is evident that in the present formulation (as in Uribe et al. [34] and Chen et al. [29]) the instantaneous SGS stresses in the filtered equation is never replaced. Instead, we only correct the mean turbulent stresses in the LES to make them consistent with the RANS results *in the average sense* as defined in Eq. (2.3). This is aligned with the other parts of the consistent hybrid framework. In particular, when $\tau_{ij}^{\text{corr}}$ in Eq. (2.11) is plugged into the modified filtered equation), the instantaneous SGS stress $\tau_{ij}^{\text{sgs}}$ and the negative of its average $-\langle\tau_{ij}^{\text{sgs}}\rangle^{\text{AVG}}$ do not cancel each other. The formulation for $\tau_{ij}^{\text{corr}}$ implicitly takes into account the mesh resolution. In regions with better mesh resolution (yet still not adequate enough to be classified as LES regions), the correction would be smaller since

https://doi.org/10.4208/cicp.220715.150416a Published online by Cambridge University Press

the resolved stress $\langle u_i'' u_j'' \rangle^{\text{AVG}}$ is larger. Only in regions where the flow has virtually no fluctuations (i.e., $\langle u_i'' u_j'' \rangle^{\text{AVG}} \approx 0$ and $\tau_{ij}^{\text{sgs}} \approx \langle \tau_{ij}^{\text{sgs}} \rangle^{\text{AVG}}$) would the formulation degenerate to a RANS turbulence model.

In the well-resolved (LES) regions the forcing terms applied on the Reynolds-averaged momentum equation and on the transport equations for the turbulent quantities are the same as in the original formulation. Hence, consistency in well-resolved (LES) regions still is explicitly enforced. However, as the new forcing $Q_i^L$ does not contain Reynolds-averaged velocity $\langle U_i \rangle^{\text{RANS}}$, solving for $\langle U_i \rangle^{\text{RANS}}$ in the entire domain is not necessary.

# 3 Dual-mesh hybrid LES/RANS framework: Implementation

## 3.1 Solver development and numerical methods

The new hybrid framework was implemented for incompressible flows based on the open source CFD platform OpenFOAM [5, 35]. The LES and RANS solvers use different meshes and they exchange information for calculating relaxation forces. To this end, first-order interpolation schemes were used to interpolate LES and RANS velocities to each other's grid, since high-order interpolations are not straightforward to implement in unstructured grids as used in OpenFOAM. Note, however, that the interpolated velocities are only used to compute the forcing terms, whose accuracies are not essential as they contain algorithmic parameters (relaxing times). The two solvers do not overwrite or manipulate each other's primary variables such as velocities. The continuity and momentum equations for incompressible turbulent flows are solved using the PISO (Pressure Implicit with Splitting of Operators) algorithm on unstructured meshes [36]. Collocated grids are used with the Rhie and Chow interpolation being employed to prevent the pressure-velocity decoupling [37]. Spatial derivatives are discretized with the finite volume method using second-order central schemes for both convection and diffusion terms. A second-order implicit time-integration scheme is used to discretize the temporal derivatives.

## 3.2 Turbulence modeling

In this hybrid framework both LES and RANS simulations are conducted simultaneously on the entire domain. For the turbulence modeling in RANS simulations, the RSTM-ER proposed by Durbin [12] is used. As discussed in Section 1, it is expected that this closure leads to better predictions in the region immediately after the separations compare to the Lauder-Sharma $k$–$\varepsilon$ model used in Xiao and Jenny [4]. This study also shows that different turbulence models (and forcing strategies) can be naturally incorporated into the current hybrid LES/RANS framework.

In the RSTM-ER turbulence model, the following equation for the Reynolds stresses

https://doi.org/10.4208/cicp.220715.150416a Published online by Cambridge University Press

is solved [12,13]:

$$\frac{\partial \tau_{ij}}{\partial t}+\frac{\partial\left(\langle U_k\rangle^{\mathrm{RANS}}\tau_{ij}\right)}{\partial x_k}=P_{ij}+\varepsilon_{ij}+D_{ij}+\mathcal{R}_{ij}, \tag{3.1}$$

where $\langle U_k\rangle^{\mathrm{RANS}}$ is the Reynolds-averaged velocity; $P_{ij}$,$\varepsilon_{ij}$, and $D_{ij}$ are turbulent stress production term, rate of dissipation term, and diffusion term, respectively. The pressure-rate-of-strain tensor $\mathcal{R}_{ij}$, which plays a critical role in the balance of Reynolds stresses and is responsible for redistributing energy among its components [13, 32], can be obtained by solving the following elliptic equation:

$$L^2\nabla^2 f_{ij}-f_{ij}=-\Pi_{ij}, \tag{3.2a}$$

$$\text{with}\quad \mathcal{R}_{ij}=k^{\mathrm{R}}f_{ij}, \tag{3.2b}$$

where $k^{\mathrm{R}}=\frac{1}{2}\tau_{ii}$ is the turbulent kinetic energy; $L$ is a length scale formulated based on $k^{\mathrm{R}}$ and $\varepsilon^{\mathrm{R}}$. The source term $\Pi_{ij}$ in the elliptic equation consists of Rotta's return-to-isotropy model and the isotropization-of-production model for quasi-homogeneous turbulence [13]. More details including the modeling of the other right-hand-side terms of the Reynolds stress equation, the coefficients, and the boundary conditions can be found in references [12,38].

The same one-equation eddy viscosity model with standard coefficients was used for SGS modeling [4]. In this model, the equation for the SGS kinetic energy $k^{\mathrm{sgs}}$ is solved [39–41]:

$$\frac{\partial k^{\mathrm{sgs}}}{\partial t}+\frac{\partial(\bar{U}_i k^{\mathrm{sgs}})}{\partial x_i}=-\tau_{ij}^{\mathrm{sgs}}\bar{S}_{ij}+\frac{\partial}{\partial x_i}\left(\nu^{\mathrm{sgs}}\frac{\partial k^{\mathrm{sgs}}}{\partial x_i}\right)-\varepsilon^{\mathrm{sgs}}, \tag{3.3a}$$

$$\text{with}\quad \tau_{ij}^{\mathrm{sgs}}-\frac{2}{3}k^{\mathrm{sgs}}\delta_{ij}=-2\nu^{\mathrm{sgs}}\left(\bar{S}_{ij}-\frac{1}{3}\bar{S}_{kk}\delta_{ij}\right), \tag{3.3b}$$

$$\nu^{\mathrm{sgs}}=C_k(k^{\mathrm{sgs}})^{1/2}\Delta, \tag{3.3c}$$

$$\text{and}\quad \varepsilon^{\mathrm{sgs}}=C_\varepsilon(k_{\mathrm{sgs}})^{3/2}\Delta^{-1}, \tag{3.3d}$$

where $\Delta$ is the filter (cell) size and $\delta_{ij}$ is the Kronecker delta. The rate-of-strain tensor $\overline{S}_{ij}$ is defined by Eq. (2.6); $C_k$ and $C_\varepsilon$ are model constants (see Ref. [4]); $\varepsilon^{\mathrm{sgs}}$ is the SGS dissipation rate; and $\nu^{\mathrm{sgs}}$ is the SGS eddy viscosity.

## 4 Numerical simulations

To appraise the performance of the modified formulation, two representative flows are tested and shown in this section, i.e., flow in a plane channel and flow over periodic hills. The main objective of the numerical simulations presented here is to illustrate the improvements resulting from the modified formulation compared to the original formulation [4]. However, since the current formulation differs from the original one by using

https://doi.org/10.4208/cicp.220715.150416a Published online by Cambridge University Press

both a different forcing strategy and a more advanced RANS model, it is important to distinguish the contributions from the two factors. Moreover, another recent improvement is the dynamic detection of LES/RANS regions based on turbulent quantities obtained on the fly [42]. A criterion based on the ratio of turbulent length scales and cell sizes was found to give encouraging results. However, the improvements resulting from dynamic LES/RANS interface detection over using pre-specified interfaces are not consistent and depend on the RANS model and the forcing strategy, particularly for the periodic hill flow, which is more complex. Therefore, in the flow over periodic hill case several combinations of RANS model, forcing strategy, and interface detection are tested to isolate their respective effects. Specifically, the effects of RANS models used in the hybrid framework are studied in Section 4.2.1, while the effects of forcing strategy and interface treatment are investigated in Section 4.2.2.

## 4.1 Flow in a plane channel at $Re_\tau = 395$

The first test case is fully developed turbulent flow in a plane channel simulated with the hybrid solver and the new forcing strategy. The domain size, meshes, and resolutions are presented in Table 1. A mesh with uniform spacing in all directions is used for the LES. The nominal Reynolds number based on friction velocity $u_\tau$ and half channel width $\delta$ is $Re_\tau = u_\tau \delta/\nu = 395$, where $u_\tau = \sqrt{\tau_w/\rho}$ and $\tau_w$ is the wall shear stress.

It is noted that the RANS mesh has more cells ($N_y = 80$) in the wall-normal direction than the LES mesh does $N_y = 60$. The reason is that in the current as well as the original framework [4], the RANS mesh is refined in the wall-normal direction to fully resolve the near-wall region, since we used low Reynolds number turbulence models without wall functions with $y^+ < 1$. On the other hand, the LES mesh only resolves the free shear flow region away from the walls and has a mesh with *uniform grid spacing* as mentioned above. Therefore, in the near-wall region the RANS mesh is indeed much finer than the LES mesh, which can lead to more cells in the RANS mesh in the wall-normal direction. For a similar reason, in the periodic hill case it is critical that the near wall region and the curvature of the hill geometry be accurately resolved, and thus we used a fine mesh for the RANS in the streamwise direction ($N_x = 128$), which is finer than the LES mesh ($N_x = 74$). However, in the statistically homogeneously direction, e.g., the spanwise direction in both cases, the RANS meshes are coarse due to the averaged nature of the RANS equations. Therefore, the overall number of cells in the RANS mesh is usually still smaller than that in the LES mesh. Also note that the time step size in RANS can be much larger, which would lead to a smaller computational cost shared by the RANS in hybrid simulations.

Non-slip boundary conditions are applied at the wall and periodic boundary conditions are imposed in the streamwise ($x$) and the spanwise ($z$) directions; the wall-normal direction is aligned with the $y$ coordinate. A uniform pressure gradient in the streamwise direction is applied to keep a constant mass flux and bulk Reynolds number. The averaging time is $T = 11\delta/U_b$ and the relaxation time for the drift terms in the RANS equations

https://doi.org/10.4208/cicp.220715.150416a Published online by Cambridge University Press

Table 1: Domain and mesh parameters for the two test cases. The $x$-, $y$-, $z$- coordinates are aligned with streamwise, wall-normal, and spanwise directions,respectively.

| cases | plane channel | periodic hill |
|---|---|---|
| domain size ($L_x \times L_y \times L_z$) | $2\pi\delta \times 2\delta \times \pi\delta$ | $9H \times 3.036H \times 4.5H$ |
| simulation time-span | $300\delta/U_b$ | $150H/U_b$ |
| $N_x \times N_y \times N_z$ (LES) | $50 \times 60 \times 30$ | $74 \times 37 \times 36$ |
| $N_x \times N_y \times N_z$ (RANS) | $10 \times 80 \times 10$ | $128 \times 37 \times 18$ |
| $\Delta x \times \Delta y \times \Delta z$ in $y^*$ (LES) | $50 \times 12 \times 41$ | $76 \times [30,72] \times 78$ (1) |
| first grid point (RANS) | $0.65y^*$ | below $2y^*$ in most areas (2) |
| time-step size | $6.68 \times 10^{-3}\delta/U_b$ | $2.8 \times 10^{-3}H/U_b$ |

(1) The numbers in the brackets indicate the range of $\Delta y$ (smallest for the cells next to the wall and largest for those at the center line). (2) The wall unit is defined as $y^* = \nu/u_\tau = \nu/\sqrt{\tau_w/\rho}$, where $\tau_w$ is the shear stress.

Table 2: Comparison of computed $Re_\tau$ (Reynolds number based on friction velocity and half channel height), which is indicative of the wall shear stress predictions.

| | $Re_\tau$ |
|---|---|
| nominal | 395 |
| DNS (reference [43]) | 392 |
| current (with RSTM-ER) | 384 |
| original (with $k$–$\varepsilon$) | 371 |
| pure LES on the same mesh | 339 |

is $T^{(R)} = 1.3\delta/U_b$; both are the same as in Xiao and Jenny [4]. In under-resolved regions the turbulent stresses in the filtered equations are corrected directly in the modified formulation. Therefore, no relaxation forcing is applied there, i.e., no relaxation time scales $T^{(L)}$ and $T^{(G)}$ are required.

The RANS region consists of all cells with distance smaller than $D_0 = 0.2\delta$ to the nearest wall. A linear ramp function $F(t)$ is multiplied on all drift terms during an initial simulation period of $2T$, where $F(0) = 0$ and $F(t \geq 2T) = 1$. This is to limit the magnitude of the drift terms during the initial period and thus to obtain better numerical stability.

Table 2 shows the Reynolds number based on shear velocity and half channel width, which corresponds to the predicted friction coefficient. Results given by the present method with RSTM as RANS model, the original method with $k-\varepsilon$ RANS model [4], and pure LES on the same mesh are compared with the DNS benchmark data. It can be seen that the present result has major improvement over the pure LES and is also better than the prediction from the original method.

The mean velocity profiles are presented in Fig. 1 in linear and semi-logarithmic scales. The streamwise velocity profiles obtained from the current hybrid solver are com-

https://doi.org/10.4208/cicp.220715.150416a Published online by Cambridge University Press

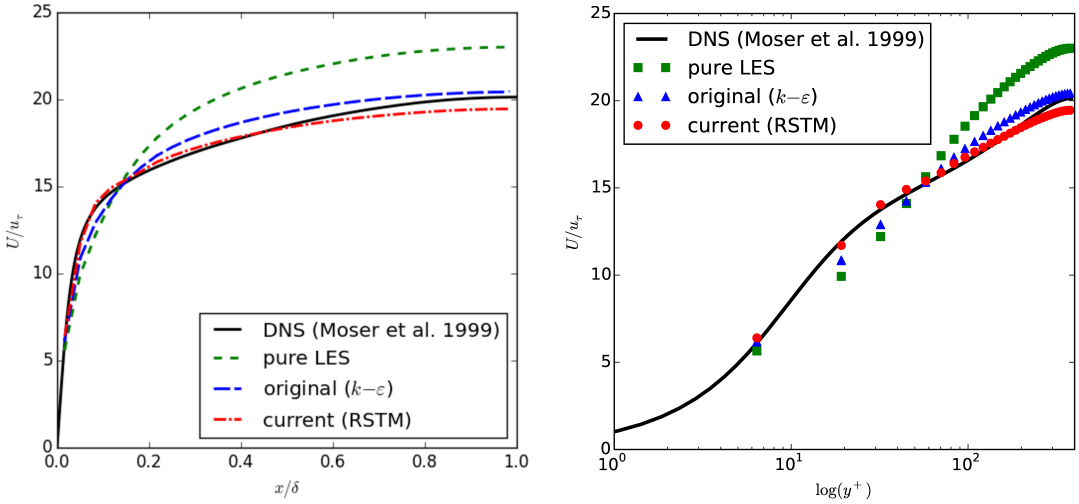



Figure 1: The mean velocity profiles of the flow in a plane channel at $Re_\tau=395$ obtained using the current and the original hybrid solver [4], the pure LES on the same mesh, and with the benchmark DNS solution of Moser et al. [43]. The velocity profiles are presented in (a) linear scale and (b) semi-logarithmic scale.

pared with the results obtained using the original formulation [4] on the same mesh, and with the benchmark DNS results of Moser et al. [43]. The comparison clearly shows that the current formulation leads to better results than the original formulation. In particular, it is noted that current results are in very good agreement with the benchmark results in the log-layer, which is due to the stress corrections applied in the near-wall region. No abnormal features are observed near the LES/RANS interface. The good agreement, however, cannot be adequately explained in the turbulent shear stress profiles shown in Fig. 2. The correction stress component $\tau_{ij}^{\text{corr}}$ is not included in the profile shown here. When that component is included, the total shear stress would move closer to the benchmark in the region between $x=0$ and 0.2 only, but other regions would remain unchanged. Based on our experiences, the hybrid methods do not give consistently good Reynolds stress predictions, even when the corresponding velocity predictions have excellent agreement with the benchmark. One possible reason is that our LES solver is based on OpenFOAM with a second order finite volume discretization based on an unstructured mesh, and thus the numerical diffusion may have played a role (i.e., by adding numerical diffusion, which can be considered an implicit Reynolds stress term). Note that in our work we deliberately used very coarse LES meshes, which is representative of scenarios in practical simulations of high Reynolds number flows. Results can be improved by refining the mesh, or using higher order numerics. However, that would lead to good results that is only possible in the low Reynolds number academic test cases, and the success would not extend to practical applications.

https://doi.org/10.4208/cicp.220715.150416a Published online by Cambridge University Press

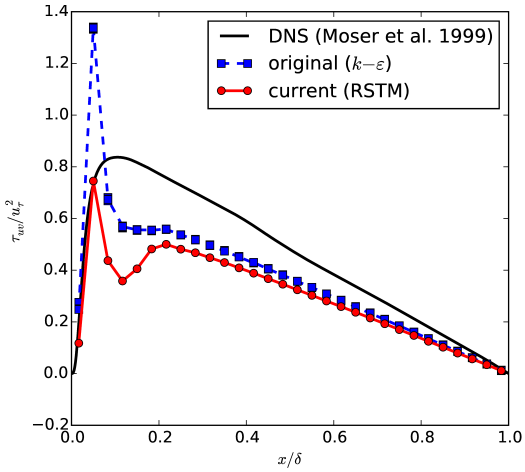



Figure 2: The total turbulent shear stresses in the plane channel flow at $Re_\tau = 395$ obtained using the current and the original hybrid solver [4] on the same mesh, compared with the benchmark DNS solution of Moser et al. [43].

## 4.2 Flow over periodic hills at $Re = 10595$

The flow over periodic hills features a massive separation and reattachment in a large part of the channel. It was chosen as a benchmark case by a French-German research group on Large-Eddy Simulation of Complex Flows [44], and Direct Numerical Simulations (DNS) and well-resolved LES were conducted for several Reynolds numbers [45, 46]. In this work, we study the case at a Reynolds number of $Re = 10595$ based on the bulk velocity $U_b$ at the hill crest and the hill height $H$, since it is more representative for practical flows. The bulk velocity was kept constant during the simulations by applying a pressure gradient on the flow. The geometry of the computational domain is shown in Fig. 3, and the detailed shape is specified using polynomials [45]. The resolutions are presented in Table 1 in each direction for the LES and RANS meshes. All length scales and coordinates presented below are normalized by the crest height $H$.

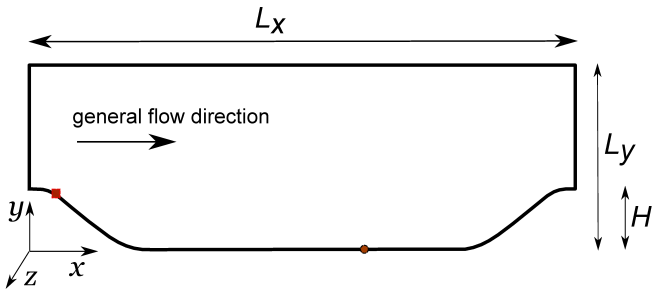
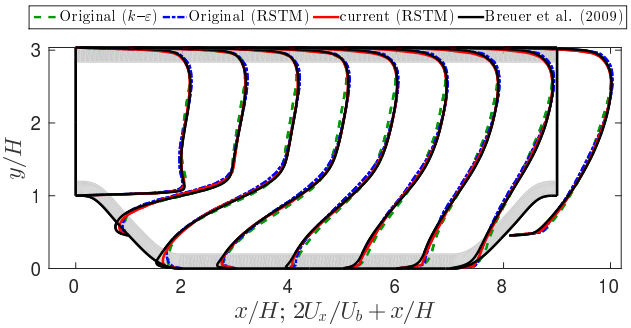



Figure 3: Schematic view of the flow over periodic hills. The dimensions of the domain are: $L_x = 9$, $L_y = 3.036$, and $L_z = 4.5$ (all normalized by the crest height $H$ of the hill). Coordinate conventions are explained in the caption of Table 1.

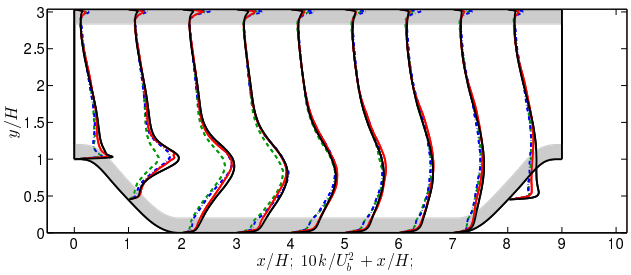
https://doi.org/10.4208/cicp.220715.150416a Published online by Cambridge University Press

### 4.2.1 Effects of using advanced RANS model (RSTM-ER)

As mentioned above, the hybrid solver employing the original relaxation forcing strategy and the Launder-Sharma $k$–$\varepsilon$ RANS model led to improved predictions compared to pure LES on a coarse mesh. During this study, we found that refining the RANS mesh in the streamwise direction further improved the results. On the other hand, when a more sophisticated RANS turbulence model such as RSTM-ER was used, no additional improvements were observed, although in pure RANS simulations the RSTM-ER performed much better than the $k$–$\varepsilon$ model. The apparent puzzle was solved by investigating the effects of the two terms ($Q_i^{(\mathrm{LU})}$, which enforces velocity consistency; and $Q_i^{(\mathrm{LG})}$, which enforces turbulent stress consistency; see Eq. (2.7)) in the relaxation force $Q_i^L$. Due to the difficulty of enforcing componentwise consistency of the turbulent stresses, the hybrid framework with the original relaxation forcing strategy is not able to fully exploit the major advantage of Reynolds stress models, i.e., the better prediction of Reynolds stresses. Furthermore, when $Q_i^{(\mathrm{LG})}$ is fully active (imposing consistency on all Reynolds stress components as opposed to enforcing consistency only in turbulent kinetic energy as in [4]), the results are worse than those obtained by enabling $Q_i^{(\mathrm{LU})}$ alone. Hence, in the



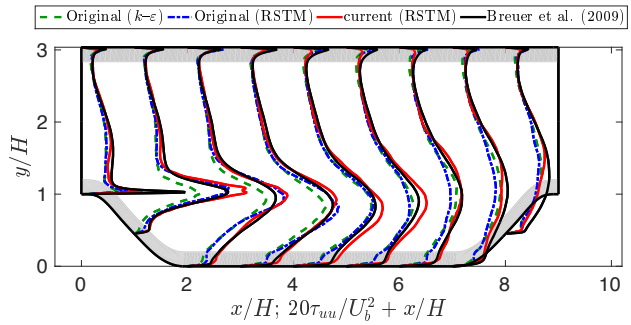

(a) Mean streamwise velocity



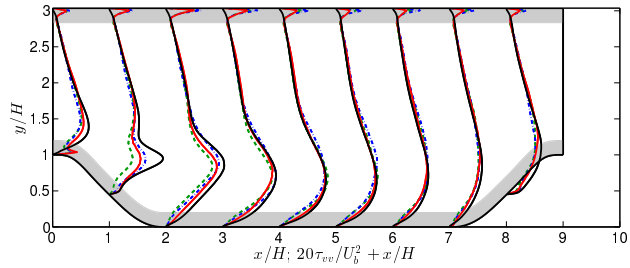

(b) Mean TKE

Figure 4: Improved predictions of mean velocity profiles and turbulent kinetic energy due to advanced RANS model and those due to the new forcing strategy. The original hybrid solver [4] with Launder-Sharma $k$–$\varepsilon$ model, that with RSTM-ER model, as well as the current hybrid solver results are compared to the benchmark solution [45]. The results with the current hybrid solver with RSTM-ER, modified forcing strategy, and dynamic LES/RANS interface is also presented and discussed in Section 4.2.2.

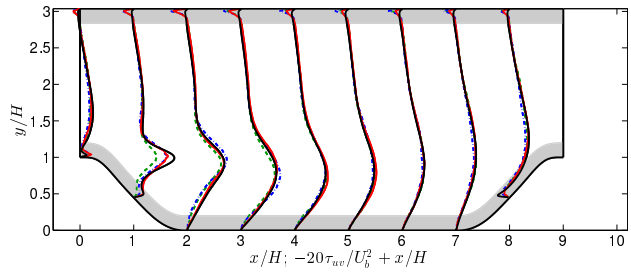
https://doi.org/10.4208/cicp.220715.150416a Published online by Cambridge University Press




(a) Mean $\tau_{uu}^{\text{LES}}$




(b) Mean $\tau_{vv}^{\text{LES}}$




(c) Mean $\tau_{uv}^{\text{LES}}$

Figure 5: Improved predictions of turbulent stresses due to advanced RANS model and those due to the new forcing strategy. See Fig. 4 for legend and detailed caption.

simulations here $Q_i^{(\text{LG})}$ is disable and only $Q_i^{(\text{LU})}$ is active. The modified forcing strategy in the current study is proposed partly to address this deficiency the original formulation associated with the $Q_i^{(\text{LG})}$ term.

Two set of simulations were performed by using the original HybridLRFoam solver with Launder-Sharma $k$–$\varepsilon$ and RSTM-ER, respectively, as RANS models, but the setups were otherwise identical. The forcing strategy and interface handing as in Ref. [4] were used. Both simulations used the RANS and LES meshes as specified in Table 1. The streamwise velocities, turbulent stresses, turbulent kinetic energy, and shear stress profile on the bottom wall are presented in Figs. 4 to 6, where the results obtained from hybrid solvers with $k$–$\varepsilon$ and RSTM-ER models are compared with the benchmark data

https://doi.org/10.4208/cicp.220715.150416a Published online by Cambridge University Press

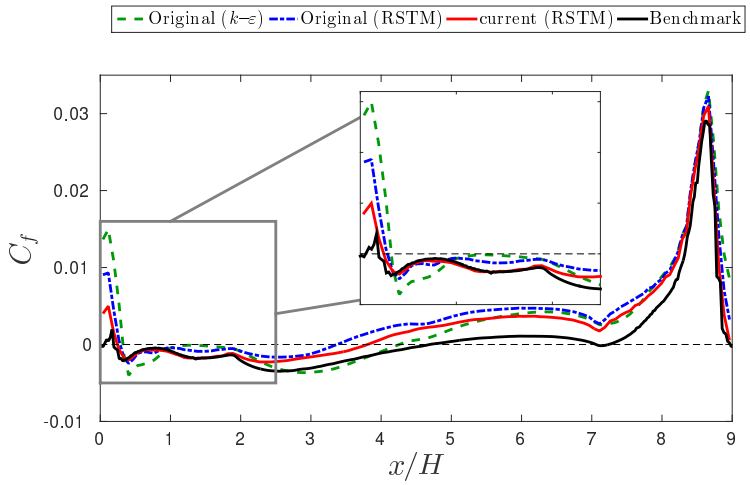
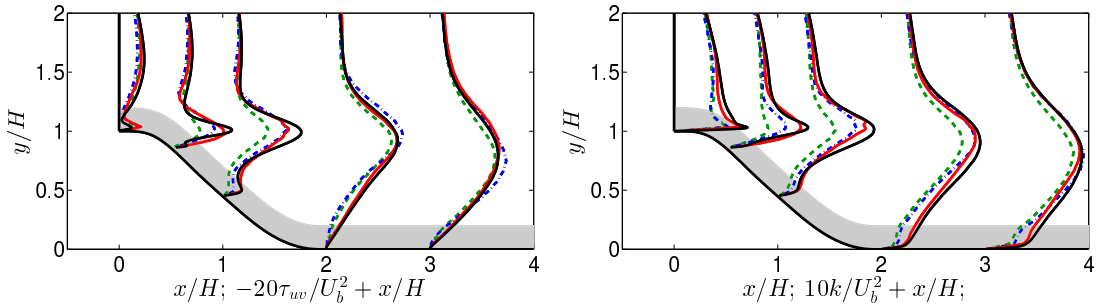



Figure 6: Improved predictions of friction coefficients $C_f = 2\tau_w/\rho U_b^2$ along the bottom wall due to advanced RANS model and those the new forcing strategy. See Fig. 4 for legend and detailed caption. The insert shows the enlargement of the region immediately after the separation.




(a) Mean $\tau_{uv}$ profiles (b) Mean TKE profiles

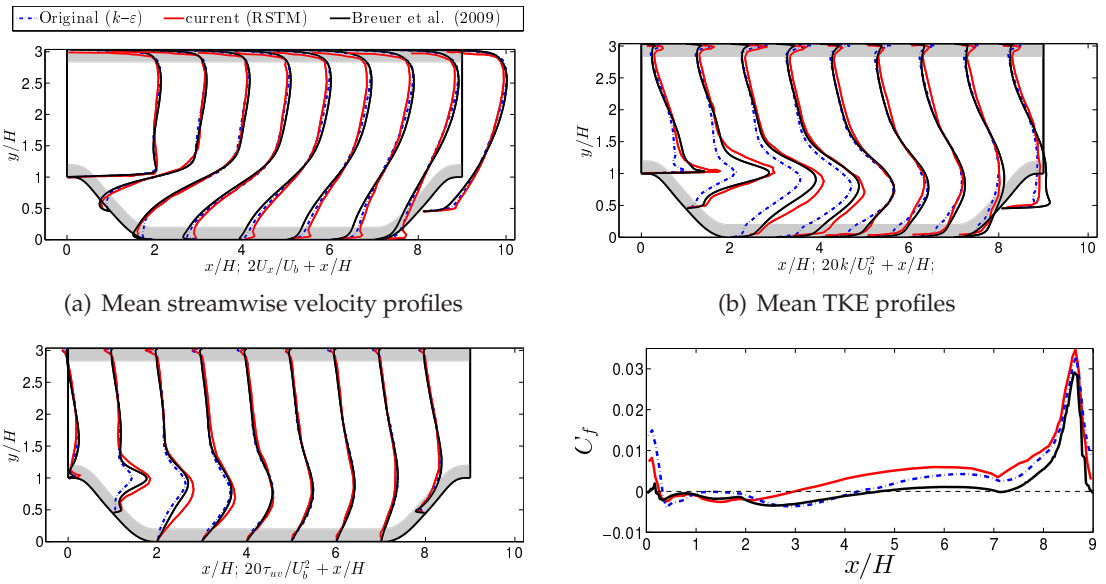
Figure 7: Zoom-in view in the separated region for $\tau_{xy}$ and $k$ in Figs. 4 and 5 with an additional profile at $x/H = 0.5$ shown.

(the results with legend "current" will be discussed separately in Section 4.2.2, and can be ignored for now). It can be seen that using a more advance RANS model does lead to improve predictions in the separated region downstream of the hill. This can only be attributed to the improved velocity predictions of the RSTM-ER RANS model in this region, since the $Q_i^{(\mathrm{LG})}$ term, which is intended to correct turbulent stresses of LES in the under-resolved region, is disabled for reasons explained above. Despite the encouraging results by using the hybrid solver with RSTM-ER RANS model, one naturally wonders whether even better predictions can be obtained by better utilizing the Reynolds stresses given by the RSTM-ER model. This is explored next by utilizing the currently proposed forcing strategy along with RSTM-ER in the hybrid solver.

https://doi.org/10.4208/cicp.220715.150416a Published online by Cambridge University Press

### 4.2.2 Effects of forcing strategy and interface handling

With the contribution of the advanced RANS model identified above, we now compare results obtained by using the hybrid solver based on the proposed forcing strategy with those from the original forcing strategy. All simulations presented here used identical LES and RANS meshes (see Table 1) as well as the same SGS and RANS models. The profiles of mean velocities, turbulent shear stresses, and wall shear stresses are displayed in Fig. 8. It can be seen that with the new forcing strategy and the RSTM-ER model the prediction quality in the separated region (between $x/H=0$ to 2) is improved dramatically, for all three quantities $U_x$, $\tau_{xy}$, and $k$. However, everywhere else and particularly in the reattached region (downstream of $x/H=4$) the results have deteriorated, which is likely due to the specified LES/RANS interface position. In Fig. 8(d) it can be seen that while the wall shear stress in separated region is better predicted, the predictions of the reattachment location and thus the shear stresses in this vicinity are much worse compared with that of the original solver. One could try specifying different LES/RANS locations, but that would be a tedious procedure, and would not be practical in actual predictions. The sensitive dependence of simulation results on LES/RANS interface locations is indeed a drawback. This observation prompted us to explore the possibility of using a dynamic forcing strategy [42].




(a) Mean streamwise velocity profiles

(b) Mean TKE profiles

(c) Mean $\tau_{uv}$ profiles

(d) Friction coefficient on the bottom wall

Figure 8: Effects of the new forcing strategy with RSTM-ER turbulence model, showing (a) streamwise velocities $U_x$, (b) turbulent kinetic energy $k$, (c) turbulent shear stress $\tau_{uv}$, and (d) shear stresses $\tau_w$ along the bottom wall, obtained with the original and current formulation with LES/RANS interfaces pre-specified as in [4]. The benchmark data of Breuer et al. [45] are used for comparison.

https://doi.org/10.4208/cicp.220715.150416a Published online by Cambridge University Press

In the results presented below, the LES/RANS interface was determined dynamically by comparing the ratio $\psi_{\min}=\min(l_x/\Delta_x, l_y/\Delta_y, l_z/\Delta_z)$ to a threshold value $\psi_0$, where $l_z$, $l_y$, and $l_z$ are the turbulent length scales in the three directions (an extension to the conventional definition of $l_t=k^{3/2}/\varepsilon$) [42], and $\Delta_x$, $\Delta_y$, $\Delta_z$ are the corresponding cell size. The length scales are estimated from the turbulent stresses and dissipation rates in the LES, both including resolved and modeled (SGS) components. A threshold value $\psi_0=2$ was chosen here.

The mean velocity profiles obtained using the current formulation, i.e., RSTM-ER RANS model, modified forcing strategy, and dynamic LES/RANS interface are compared with those obtained using original relaxation forcing, the benchmark results of Breuer et al. [45], and the results presented in Section 4.2.1. It can be seen that predictions from all formulations almost perfectly match the benchmark results in most areas. A minor exception is that the original forcing together with the $k$–$\varepsilon$ turbulent model is not able to accurately capture the recirculation immediately after the separation (most visible at $x/H=2$). This is not *directly* related to the different forcing strategies, but related to the deficiency of the two-equation models in predicting flows with recirculations. Compared to the results of original hybrid solver with RSTM-ER model, the current results lead to further improvement in the separated region, as is evident from Fig. 4(b) (also see Fig. 7 for a detailed view and additional profiles in the separated region at $x/H=0.5$.)

The turbulent kinetic energy and three components of the turbulent stresses $\tau_{uv}^{\text{LES}}$, $\tau_{uu}^{\text{LES}}$, $\tau_{vv}^{\text{LES}}$ obtained with the current solver are shown in Fig. 5 at nine streamwise locations. All these second-moment quantities include both the resolved part and the modeled (SGS) part, as defined in Eq. (2.5). The profiles shown here represent temporal and spanwise averaged quantities. From the plots of all these quantities it can be observed that the two simulations lead to equally good predictions near and after the reattachment point (at approximately $x/H=4$). This is expected, since $k$–$\varepsilon$ models are known to perform well for attached flows. However, in the recirculation region and particularly in the region immediately after separation (between $x/H=1$ and 2), the new strategy based on the RSTM-ER leads to much better results. This is due to better predictions of RSTM-ER in this region. In this hybrid framework, the RANS solver based on the Reynolds stress transport model gives significantly improved turbulent stress predictions, which are then used to correct the corresponding term in the filtered equations.

The wall shear stresses are shown in Fig. 6. Again, all the hybrid simulations perform similarly in the attached flow regions. The original consistent forcing strategy with $k$–$\varepsilon$ model does a slightly better job near the reattachment point (near $x/H=4.5$). However, the wall shear stresses in the separated flow region (between $x/H=0$ and 4) are predicted much better with the new formulation based on RSTM-ER.

Finally, since the LES/RANS regions are determined dynamically based on turbulent quantities obtained during the simulations, it is of interest to see which cells are classified as under-resolved and have a nonzero turbulent stress correction $\tau_{ij}^{\text{corr}}$ or, equivalently, a nonzero correction force $Q_i^{\text{LES}}$ in the momentum equation. In Fig. 9 the magnitude $|\mathbf{Q}^L|$ of

https://doi.org/10.4208/cicp.220715.150416a Published online by Cambridge University Press

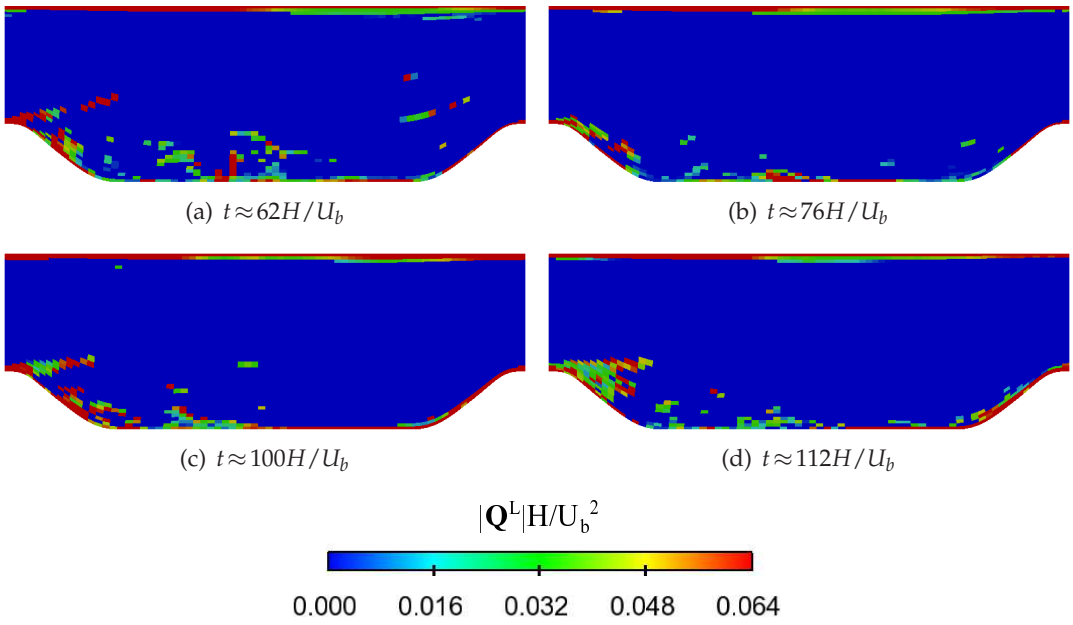



Figure 9: Instantaneous snapshots of the direct forcing magnitude $|\mathbf{Q}^L|$ at four time instances, normalized by $U_b^2/H$. This forcing is non-zero only in the under-resolved cells as determined by a criterion based on ratio of the turbulent length-scale and the cell size.

the forcing $Q_i^{\text{LES}}$ normalized by $U_b^2/H$ is shown at four time instances. The normalization factor is indicative of inertial forces magnitude. The four snapshots in this figure suggest that the correction force is spatially and temporally intermittent in the region immediately downstream of the hill crest. As such, a mean LES/RANS interface is difficult to specify and would not be informative either, which is why the instantaneous snapshots are shown here. The cells with $Q_i^{\text{LES}} = 0$ are mostly well-resolved (LES) ones, obtained from indicators comparing turbulent length scales and cell sizes. Note, however, that the instantaneous LES/RANS cell indicators are obtained from turbulent length scales that are based on exponentially averaged LES velocities. Therefore, their fluctuations should be at a much lower frequency than the LES velocity themselves, and should instead be comparable to the RANS velocities fluctuation frequencies. Furthermore, it can be seen from Fig. 9 that the under-resolved region as determined by the turbulent length scale criterion is thick in the recirculation region, thinner near the top wall, and thinnest along the bottom wall in the reattached region. It is not guaranteed that this is the best way to classify LES/RANS regions. However, the RSTM-ER typically has good performance in modeling separated flows and recirculations, and in the near-wall region the hybrid solver with the new forcing strategy together with RSTM-ER is robust regarding LES/RANS interface locations. This seems to justify observed LES/RANS interfaces.

In summary, from the mean velocity profiles, the Reynolds stress profiles, and the

https://doi.org/10.4208/cicp.220715.150416a Published online by Cambridge University Press

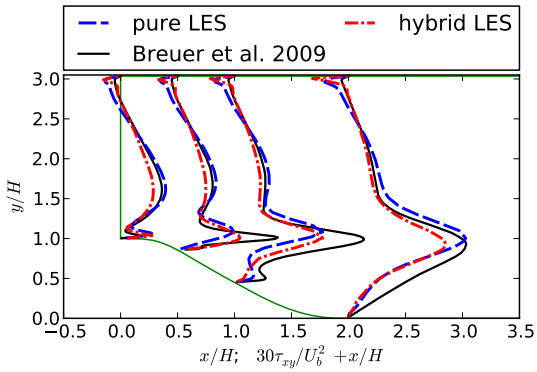
shear stress along the bottom wall we reach the following conclusions: (1) in the reattached flow region a RANS solver with the Launder-Sharma $k$–$\varepsilon$ model is adequate as a component of the hybrid solver; and (2) in the separated region the hybrid solver with RSTM-ER leads to significantly better results.

### 4.3 Comparison with original HybridLRFoam and ImpactFoam

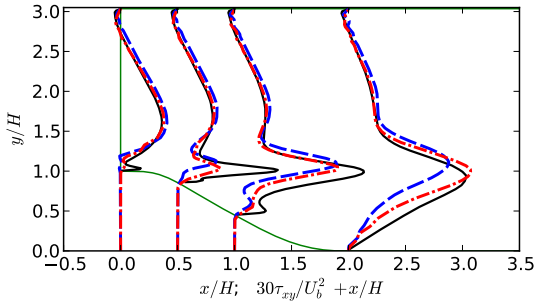
As mentioned in Section 1, Xiao et al. [7] and the current work represent two individual attempts to improve the original hybrid LES/RANS solver developed in [4]. Xiao et al. [7] tried to improve the prediction quality by using a high-order, high-accuracy in-house LES solver. In contrast, this work attempts to use a more advanced RANS model and a different forcing strategy. The main motivation in this approach is to improve the prediction of flow with separations. As such, it is not illustrative to compare the ImpactFoam results in [7] and the current results directly. After all, in the two solvers the improvements are due to distinct factors, i.e., improved LES solver for ImpactFoam, and improved RANS model and forcing strategy for current results. Indeed, even with the original forcing strategy and Launder-Sharma $k$–$\varepsilon$ model, the ImpactFoam results are comparable to the current results in most locations. This is evident from Fig. 10(b), where the hybrid simulation results of turbulent shear stresses and turbulent kinetic energy are presented for the original HybridLRFoam [4], ImpactFoam, and HybridLRFoam with the current formulation. However, to highlight the effects of the more advanced RANS model and forcing strategy used in the current formulation, we should compare not the prediction quality of the hybrid solvers but the *improvements* over the corresponding pure (under-resolved) LES results for the three solvers. Only the separated flow region is shown in Fig. 10, since all three solvers perform equally well in other regions, and the purpose of the current formulation is to address the deficiency of the original hybrid solver in separated flow regions. It can be seen that for the original HybridLRFoam solver and the ImpactFoam solver, the improvements in the separated region are negligible. Particularly at $x/H=0.5$ and 1, the hybrid solver predictions are similar to or even worse than the pure LES results, although in the case of impactFOAM the pure LES results are better than those in the two HybridLRFoam cases due to the high-order LES solver used in the former. This trend is very consistent for the turbulent kinetic energy and among all components of the turbulent stresses $\tau_{ij}$ (for brevity only $\tau_{uv}$ is shown). In contrast, the current HybridLRFoam solver leads to clearly improved predictions for all streamwise locations, particularly at $x/H=0.5$ and 1. This observation shows that current hybrid solver with advanced RANS model and the modified forcing strategy indeed performs better in the separated region, in that they lead to more improvements compared to the corresponding pure LES results.

Regarding the prediction shear stresses on the bottom wall, an important difference for the ImpactFoam results is that the wall shear stresses shown in Ref. [7] are RANS results, and not from the LES solver. This is because the LES solver is based on a Cartesian mesh instead of body-fitting mesh, and thus it is not straightforward to obtain wall shear

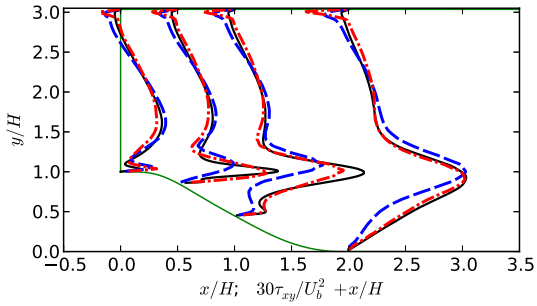
https://doi.org/10.4208/cicp.220715.150416a Published online by Cambridge University Press




(a) $\tau_{uv}$, HybridLRFoam (original), $k$–$\varepsilon$




(b) $\tau_{uv}$, ImpactFoam, $k$–$\varepsilon$




(c) $\tau_{uv}$, HybridLRFoam (current), RSTM-ER

Figure 10: Improved predictions of turbulent shear stresses $\tau_{uv}$ in hybrid simulations compared with corresponding pure LES results, showing the results from (a) HybridLRFoam [4], the original hybrid solver with OpenFOAM RANS and LES solvers; (b) ImpactFoam [7], a hybrid solver with the same forcing strategy and RANS solver as in (a) but with a high-order, high-accuracy in-house LES solver; and (c) HybridLRFoam with current formulation, which has the same LES solver as in (a) but with an advanced RSTM-ER RANS solver, a modified forcing strategy, and dynamic LES/RANS interface detection.

stress in the LES solver. Therefore, the results obtained there is not completely comparable to the current results. Accordingly, the comparison of wall shear stresses was made between RANS results in the original formulation and RANS results in ImpactFoam (see the legend of Fig. 10 in Ref. [7]). Despite the differences, we point out that the current

https://doi.org/10.4208/cicp.220715.150416a Published online by Cambridge University Press

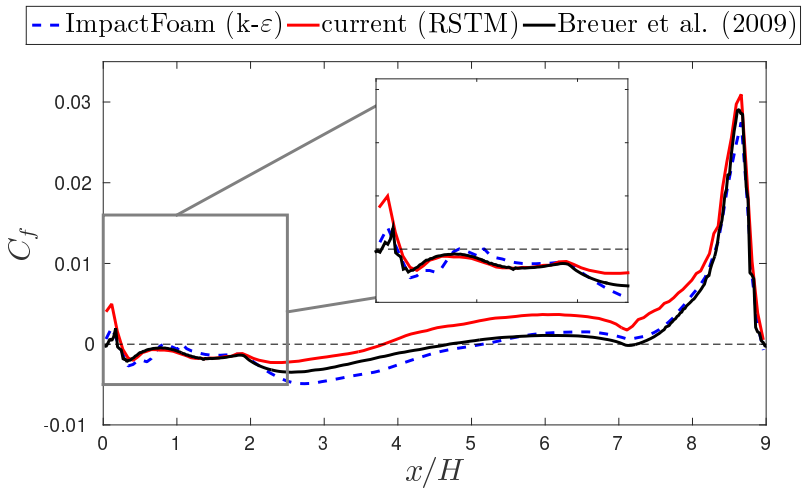



Figure 11: Comparison of the wall shear stress prediction on the bottom wall from ImpactFoam [7] and that from the current hybrid solver.

prediction of wall shear stress prediction is very good and is of similar quality to that of the RANS solver in ImpactFoam, which is shown in Fig. 11.

## 5 Discussion

The dual-mesh and dual-solver configuration is an important feature of the hybrid LES/RANS framework proposed in Xiao and Jenny [4]. The modified formulation of the hybrid framework inherits this feature. Thanks to the dual-solver configuration, the hybrid framework is weakly intrusive in the sense that the LES and RANS solvers are relatively independent, i.e., exchange of information between the two solvers and meshes only occurs through (relaxation or direct) forcing terms. This leads to the following advantages:

(i) This formulation makes it possible to develop a hybrid solver based on established LES and RANS models, for example by combining selections from high-order academic solvers, black-box commercial solvers, and flexible open-source or in-house solvers, as long as both solvers allow the user to add force terms to the momentum and continuity equations and to access fields (e.g., velocities and stresses) during the simulations. For example, using an in-house high-order LES solver and a general-purpose RANS solver is a reasonable choice, which combines the accuracy and efficiency of the former with the mesh flexibility of the latter [7].

(ii) A coupled solver can be developed by writing a high-level driver script to call an LES and a RANS model as independent modules. This can be a desirable feature in industrial simulations, where many solvers are used for different purposes (e.g., preliminary evaluation, design, and optimization).

https://doi.org/10.4208/cicp.220715.150416a Published online by Cambridge University Press

(iii) Different time step sizes can be used in the LES and the RANS simulations. Usually the time step size for the RANS simulation can be much larger than that used in LES for the same flow, which reduces the computational overhead due to performing RANS simulation in addition to the LES.

(iv) The LES and RANS solvers may communicate via files on disks or variables in memory depending on the specific scenario. Communicating via files is feasible if the time step of the RANS solver is large and communication is infrequent.

(v) The LES and RANS solvers in the hybrid framework can directly make use of whatever turbulence models available in the respective standalone solvers with only few code modifications.

We believe that these advantages are all important from a software engineering perspective. Admittedly, they are achieved at the expense of running two solvers for the same problem, which also adds more complexity to the simulation setup.

The different natures of LES and RANS simulations also lead to different requirements for the LES and RANS meshes. In the hybrid solver, the LES mesh only needs to be refined in the regions where interesting features develop (e.g., the wake region behind a cylinder or airfoil), while the RANS mesh only needs to be refined near the wall in the wall-normal direction. We believe that these meshes with single-objective refinements are easier to generate than the meshes that need refinements in various regions. This is particularly true for generating locally-structured, globally-unstructured meshes (where the domain is divided into many arbitrarily connected blocks, each consisting of a structured mesh), which are usually preferred for practical simulations whenever possible. On the other hand, one could also argue that it is difficult enough to generate one mesh for a domain with a complex geometry and that the additional mesh needed in the hybrid solver poses an extra hurdle for the users (Menter 2011, private communication).

For the modified formulation the dual-mesh dual-solver configuration can be avoided since the averaged filtered velocity $\langle\overline{U}_i\rangle^{\mathrm{AVG}}$ does not explicitly relax towards the Reynolds-averaged velocity $\langle U_i\rangle^{\mathrm{RANS}}$, one could choose not to solve the extra RANS momentum and continuity equations, but simply take $\langle U_i\rangle^{\mathrm{AVG}}$ as the RANS velocity. This single-solver strategy is used in the work of Uribe et al. [34]. This approach guarantees the velocity consistency and the average velocity $\langle U_i\rangle^{\mathrm{AVG}}$ is used in the transport equations for turbulent quantities such as $\tau_{ij}$ and $\varepsilon^{\mathrm{R}}$.

Even if no RANS equation is solved directly, the transport equations for $\tau_{ij}$ and $\varepsilon^{\mathrm{R}}$ still need to be solved. One has the choice of solving them on a separate RANS mesh or on the same mesh used for the LES. The former choice leads to a *single-solver dual-mesh* configuration and the latter to *single-solver single-mesh* configuration. In the single-solver single mesh case, the mesh must be adequate for LES far from the wall and suitable for RANS in the near-wall region, which adds a constraint on the meshing process similar in DES [47]. The results presented in this work were obtained with the dual-mesh dual-solver configuration. However, modifying the current solver to obtain a single-solver

https://doi.org/10.4208/cicp.220715.150416a Published online by Cambridge University Press

and/or single-mesh configuration is straightforward. It can be achieved by disabling the solution procedure for RANS momentum and continuity equations ($\langle U_i\rangle^{\text{RANS}}$ and $\langle p\rangle^{\text{RANS}}$), directly set $\langle U_i\rangle^{\text{RANS}}$ to the averaged filtered velocity field $\langle \overline{U}_i\rangle^{\text{AVG}}$, and use the same mesh for LES and RANS simulations. Hence, the presented hybrid solver offers more flexibility to choose between single- and dual-solver, and between single- and dual-mesh configurations.

## 6 Conclusions

The consistent hybrid LES/RANS framework previously proposed by Xiao and Jenny [4] has been modified to better exploit the advantages offered by more advanced RANS models with better Reynolds stress prediction, such as the Reynolds stress transport model by Durbin [12]. In the new formulation the LES turbulent stresses are directly modified in the under-resolved regions, which is in contrast to the original strategy, where the consistency between velocities and turbulent stresses in LES and RANS simulations are enforced via relaxation terms. As in the previously presented hybrid framework, the different interpretations of filtered and Reynolds-averaged quantities are accounted for by employing an exponentially weighted averaging to estimate Reynolds averages from the LES solution.

The modified strategy is evaluated for a plane channel flow and flow over periodic hills. An appreciable improvement over the results obtained with the original relaxation forcing strategy can be observed from the mean profiles of velocity, turbulent stresses, and wall shear stresses. In the plane channel case, the superiority seems to be due to the fact that the new formulation directly modifies the turbulent stresses. In the flow over periodic hill test case the improvements are most obvious in the region immediately after the separation, which are attributed to the advanced Reynolds stress transport model used in the hybrid solver as well as the new formulation's capability to take advantage of the better Reynolds stress predictions offered by the more advanced model. The individual contributions from the two components are identified.

In summary, the modified formulation of the hybrid framework represents an effective, feasible, and robust way to overcome the difficulty with the original relaxation forcing of enforcing componentwise Reynolds stress consistency. Preliminary evaluations with two representative cases show promising results.

## Acknowledgments

HX would like to acknowledge the financial support from the Commission for Technology and Innovation (CTI) of Switzerland. The computational resources used for this project were provided by ETH Zürich, which are gratefully acknowledged.

https://doi.org/10.4208/cicp.220715.150416a Published online by Cambridge University Press

## Appendix: Derivation of direct forcing $Q_L$ in filtered equations

The derivation below follows that of Chen et al. [25], although our reasoning, assumptions, and implementations are different. Our derivation is presented here for completeness.

Taking the averaging of the filtered momentum equation

$$\frac{\partial \overline{U}_i}{\partial t}+\frac{\partial(\overline{U}_i\overline{U}_j)}{\partial x_j}=-\frac{1}{\rho}\frac{\partial \overline{p}}{\partial x_i}+\nu\frac{\partial^2\overline{U}_i}{\partial x_j\partial x_j}-\frac{\partial \tau_{ij}^{\rm sgs}}{\partial x_j}, \tag{A.1}$$

by using the stationary turbulence approximation, the definition in Eq. (2.4), and the property of the averaging operation in Eq. (2.12c), we have

$$\begin{aligned}&\frac{\partial\langle\overline{U}_i\rangle^{\rm AVG}}{\partial t}+\frac{\partial}{\partial x_j}\left[\langle\overline{U}_i\rangle^{\rm AVG}\langle\overline{U}_j\rangle^{\rm AVG}+\langle u_i''u_j''\rangle^{\rm AVG}\right]\\ =&-\frac{1}{\rho}\frac{\partial\langle\overline{p}\rangle^{\rm AVG}}{\partial x_i}+\nu\frac{\partial^2\langle\overline{U}_i\rangle^{\rm AVG}}{\partial x_j\partial x_j}-\frac{\partial}{\partial x_j}\left(\langle\tau_{ij}^{\rm sgs}\rangle^{\rm AVG}\right).\end{aligned} \tag{A.2a}$$

or equivalently:

$$\begin{aligned}\frac{\partial\langle\overline{U}_i\rangle^{\rm AVG}}{\partial t}+\frac{\partial(\langle\overline{U}_i\rangle^{\rm AVG}\langle\overline{U}_j\rangle^{\rm AVG})}{\partial x_j}=&-\frac{1}{\rho}\frac{\partial\langle\overline{p}\rangle^{\rm AVG}}{\partial x_i}+\nu\frac{\partial^2\langle\overline{U}_i\rangle^{\rm AVG}}{\partial x_j\partial x_j}\\ &\underbrace{-\frac{\partial}{\partial x_j}\left(\langle\tau_{ij}^{\rm sgs}\rangle^{\rm AVG}+\langle u_i''u_j''\rangle^{\rm AVG}\right)}_{\text{turbulent stress term}}.\end{aligned} \tag{A.2b}$$

Note that the resolved turbulent stress term $\langle u_i''u_j''\rangle^{\rm AVG}$ can be explicitly computed from $\overline{U}_i$ by using the definition of $\langle\cdot\rangle^{\rm AVG}$ and $u_i''$ as in Eqs. (2.2) and (2.4), respectively.

On the other hand, the RANS momentum equation reads

$$\frac{\partial\langle U_i\rangle^{\rm RANS}}{\partial t}+\frac{\partial(\langle U_i\rangle^{\rm RANS}\langle U_j\rangle^{\rm RANS})}{\partial x_j}=-\frac{1}{\rho}\frac{\partial\langle p\rangle^{\rm RANS}}{\partial x_i}+\nu\frac{\partial^2\langle U_i\rangle^{\rm RANS}}{\partial x_j\partial x_j}\underbrace{-\frac{\partial\tau_{ij}}{\partial x_j}}_{\text{Reynolds stress term}}. \tag{A.3}$$

Comparing Eqs. (A.2) and (A.3) it can be seen that the consistency between $\langle\overline{U}_i\rangle^{\rm AVG}$ and $\langle U_i\rangle^{\rm RANS}$ can be achieved by requiring consistency between the turbulent stresses. This is enforced by correcting the turbulent stress term in Eq. (A.2) in the under-resolved regions only according to the Reynolds stress term in Eq. (A.3), i.e., by modifying Eq. (A.2) as follows:

$$\begin{aligned}\frac{\partial\langle\overline{U}_i\rangle^{\rm AVG}}{\partial t}+\frac{\partial(\langle\overline{U}_i\rangle^{\rm AVG}\langle\overline{U}_j\rangle^{\rm AVG})}{\partial x_j}=&-\frac{1}{\rho}\frac{\partial\langle\overline{p}\rangle^{\rm AVG}}{\partial x_i}+\nu\frac{\partial^2\langle\overline{U}_i\rangle^{\rm AVG}}{\partial x_j\partial x_j}\\ &-\frac{\partial}{\partial x_j}\left[\langle\tau_{ij}^{\rm sgs}\rangle^{\rm AVG}+\langle u_i''u_j''\rangle^{\rm AVG}+\tau_{ij}^{\rm corr}\right]\end{aligned} \tag{A.4}$$

https://doi.org/10.4208/cicp.220715.150416a Published online by Cambridge University Press

with $\tau_{ij}^{\text{corr}}$ being the only additional term, which is defined in Eq. (2.11).

It can be seen that according to Eq. (A.4) it is desirable to change the filtered equation (A.1) to the following form:

$$\frac{\partial \overline{U}_i}{\partial t}+\frac{\partial(\overline{U}_i\overline{U}_j)}{\partial x_j}=-\frac{1}{\rho}\frac{\partial \overline{p}}{\partial x_i}+\nu\frac{\partial^2\overline{U}_i}{\partial x_j\partial x_j}-\frac{\partial}{\partial x_j}\left(\tau_{ij}^{\text{sgs}}+\tau_{ij}^{\text{corr}}\right) \tag{A.5a}$$

or equivalently

$$\frac{\partial \overline{U}_i}{\partial t}+\frac{\partial(\overline{U}_i\overline{U}_j)}{\partial x_j}=-\frac{1}{\rho}\frac{\partial \overline{p}}{\partial x_i}+\nu\frac{\partial^2\overline{U}_i}{\partial x_j\partial x_j}-\frac{\partial \tau_{ij}^{\text{sgs}}}{\partial x_j}+Q_i^{\text{L}} \tag{A.5b}$$

with $Q_i^{\text{L}}$ and $\tau_{ij}^{\text{corr}}$ defined in Eqs. (2.10) and (2.11), respectively. This way, averaging the modified filtered equation (A.5) would lead to Eq. (A.2), which is consistent with the RANS counterpart Eq. (A.3). Note that under the stationary turbulence approximation, $\langle\tau_{ij}^{\text{corr}}\rangle^{\text{AVG}}$ is equivalent to $\tau_{ij}^{\text{corr}}$ since it is formulated based on averaged quantities; see Eq. (2.11).

## References


[1] U. Piomelli and E. Balaras. Wall-layer models for large-eddy simulations. *Annual Review of Fluid Mechanics*, 34:349–374, 2002.

[2] D. R. Chapman. Computational aerodynamics: development and outlook. *AIAA Journal*, 17: 1293–313, 1979.

[3] H. Choi and P. Moin. Grid-point requirements for large eddy simulation: Chapman's estimates revisited. *Physics of Fluids*, 24(1):011702, 2012.

[4] H. Xiao and P. Jenny. A consistent dual-mesh framework for hybrid LES/RANS modeling. *Journal of Computational Physics*, 231(4):1848–1865, 2012.

[5] OpenCFD Ltd. The open source CFD toolbox. URL: http://www.openfoam.com, 2011.

[6] H. Xiao, M. Wild, and P. Jenny. Preliminary evaluation and applications of a consistent hybrid LES–RANS method. In S. Fu, editor, *Notes on Numerical Fluid Mechanics and Multidisciplinary Design*, 117. Springer, 2012.

[7] H. Xiao, Y. Sakai, R. Heninger, M. Wild, and P. Jenny. Coupling of solvers with non-conforming computational domains in a dual-mesh hybrid LES/RANS framework. *Computers and Fluids*, 88, 2013.

[8] R. Henninger. IMPACT simulation code. URL `\url{http://www.ifd.mavt.ethz.ch/research/group_lk/projects/impact}`. Retrieved July 2012.

[9] R. Henniger, D. Obrist, and L. Kleiser. High-order accurate solution of the incompressible Navier–Stokes equations on massively parallel computers. *Journal of Computational Physics*, 229(10):3543–3572, 2010.

[10] B. E. Launder and B. I. Sharma. Application of the energy-dissipation model of turbulence to the calculation of flow near a spinning disc. *Letters in Heat and Mass Transfer*, 1(2):131–138, 1974.

[11] F. Billard. *Development of a robust elliptic-blending turbulence model for near-wall, separated and buoyant flows*. PhD thesis, University of Manchester, 2011. Chapter 6.

[12] P. A. Durbin. A Reynolds stress model for near-wall turbulence. *Journal of Fluid Mechanics*, 249:465–498, 1993a.


https://doi.org/10.4208/cicp.220715.150416a Published online by Cambridge University Press

[13] B.E. Launder, G.J. Reece, and W. Rodi. Progress in development of a Reynolds-stress turbulence closure. *Journal of Fluid Mechanics*, 68:537–566, 1975.
[14] R. Manceau and K. Hanjalic. A new form of the elliptic relaxation equation to account for wall effects in RANS modeling. *Physics of Fluids*, 12(9):2345–2351, 2000.
[15] R. Manceau and K. Hanjalic. Elliptic blending model: A new near-wall Reynolds-stress turbulence closure. *Physics of Fluids*, 14(2):744–754, 2002.
[16] V. Wizman, D. Laurence, M. Kanniche, P. Durbin, and A. Demuren. Modeling near-wall effects in second-moment closures by elliptic relaxation. *International Journal of Heat and Fluid Flow*, 17(3):255–266, 1996.
[17] B.A. Pettersson and H.I. Andersson. Near-wall Reynolds-stress modelling in noninertial frames of reference. *Fluid Dynamics Research*, 19(5):251–276, 1997.
[18] P. R. Spalart, W. H. Jou, M. Strelets, and S. R. Allmaras. Comments on the feasibility of LES for wings, and on a hybrid RANS/LES approach. In *First AFOSR International Conference on DNS/LES*. Greyden Press, Ruston, Louisiana, August 1997.
[19] S. S. Girimaji. Partially-averaged Navier-Stokes model for turbulence: A Reynolds-averaged Navier-Stokes to direct numerical simulation bridging method. *Journal of Applied Mechanics*, 73(3):413, 2006.
[20] R. Schiestel and A. Dejoan. Towards a new partially integrated transport model for coarse grid and unsteady turbulent flow simulations. *Theoretical and Computational Fluid Dynamics*, 18(6):443–468, 2004.
[21] A. Fadai-Ghotbi, C. Friess, R. Manceau, and J. Boree. A seamless hybrid RANS–LES model based on transport equations for the subgrid stresses and elliptic blending. *Physics of Fluids*, 22(5):055104, 2010.
[22] R. Schiestel. Multiple-time-scale modeling of turbulent flows in one-point closures. *Physics of Fluids*, 30(3):722, 1987.
[23] P. Sagaut, S. Deck, and M. Terracol. *Multiscale and Multiresolution Approaches in Turbulence*. Imperial College Press, 2006.
[24] C. Speziale. Turbulence modeling for time-dependent RANS and VLES: A review. *AIAA Journal*, 36:173–184, 1998.
[25] S. Chen, Z. Xia, S. Pei, J. Wang, Y. Yang, Z. Xiao, and Y. Shi. Reynolds-stress-constrained large-eddy simulation of wall-bounded turbulent flows. *Journal of Fluid Mechanics*, 703:1–28, 2012.
[26] Y. Shi, Z. Xiao, and S. Chen. Constrained subgrid-scale stress model for large eddy simulation. *Physics of Fluids*, 20(1):011701, 2008.
[27] J. Fröhlich and D. von Terzi. Hybrid LES/RANS methods for the simulation of turbulent flows. *Progress in Aerospace Sciences*, 44(5):349–377, 2008.
[28] J. S. Baggett. On the feasibility of merging LES with RANS for the near-wall region of attached turbulent flows. In *Annual Research Briefs*, pages 267–277. Center for Turbulence Research, 1998.
[29] S. Chen, Y. Chen, Z. Xia, K. Qu, Y. Shi, Z. Xiao, Q. Liu, Q. Cai, F. Liu, C. Lee, et al. Constrained large-eddy simulation and detached eddy simulation of flow past a commercial aircraft at 14 degrees angle of attack. *Science China: Physics, Mechanics and Astronomy*, 56(2): 270–276, 2013.
[30] Z. Xia, Y. Shi, R. Hong, Z. Xiao, and S. Chen. Constrained large-eddy simulation of separated flow in a channel with streamwise-periodic constrictions. *Journal of Turbulence*, 14(1):1–21, 2013.
[31] Q. Xu and Y. Yang. Reynolds stress constrained large eddy simulation of separation flows

https://doi.org/10.4208/cicp.220715.150416a Published online by Cambridge University Press

in a U-duct. *Propulsion and Power Research*, 3(2):49–58, 2014.
[32] S. B. Pope. *Turbulent Flows*. Cambridge University Press, Cambridge, 2000.
[33] P. R. Spalart and S. R. Allmaras. A one-equation turbulence model for aerodynamic flows. In *Proceedings of the 30th Aerospace Sciences Meeting and Exibit*. AIAA, January 6-9 1992. Paper number: AIAA-92-0439.
[34] J. C. Uribe, N. Jarrin, R. Prosser, and D. Laurence. Development of a two-velocities hybrid RANS–LES model and its application to a trailing edge flow. *Flow Turbulence Combustion*, 85 (2):181–197, 2010.
[35] H. G. Weller, G. Tabor, H. Jasak, and C. Fureby. A tensorial approach to computational continuum mechanics using object-oriented techniques. *Computers in Physics*, 12(6):620–631, 1998. doi: 10.1063/1.168744.
[36] R. I. Issa. Solution of the implicitly discretised fluid flow equations by operator-splitting. *Journal of Computational Physics*, 62:40–65, 1986.
[37] C. M. Rhie and W. L. Chow. A numerical study of the turbulent flow past an isolated airfoil with trailing edge separation. *AIAA*, 21(11):1525–1532, 1983.
[38] P. Durbin. Application of a near-wall turbulence model to boundary layers and heat transfer. *International Journal of Heat and Fluid Flow*, 14(4):316–323, 1993b.
[39] A. Yoshizawa and K. Horiuti. A statistically-derived subgrid-scale kinetic energy model for the large-eddy-simulation of turbulent flows. *Journal of Physical Society of Japan*, 54:2834–2839, 1985.
[40] K. Horiuti. Large eddy simulation of turbulent channel flow by one-equation modeling. *Journal of the Physical Society of Japan*, 54:2855–2865, 1985.
[41] C. Fureby, G. Tabor, H. G. Weller, and A. D. Gosman. Comparative study of subgrid scale models in homogeneous isotropic turbulence. *Physics of Fluids*, 9(5), 1997.
[42] H. Xiao and P. Jenny. Dynamic evaluation of mesh resolution in hybrid LES/RANS methods. *Flow, Turbulence and Combustion*, 93, 2014.
[43] R. D. Moser, J. D. Kim, and N. N. Mansour. Direct numerical simulation of turbulent channel flow up to $Re_\tau$=590. *Physics of Fluids*, 11:943–945, 1999.
[44] S. Saric, S. Jakirlic, M. Breuer, B. Jaffrezic, G. Deng, O. Chikhaoui, J. Fröhlich, D. von Terzi, M. Manhart, and N. Peller. Evaluation of detached eddy simulations for predicting the flow over periodic hills. In *ESAIM: Proceedings*, volume 16, pages 133–145, 2007. doi: 10.1051/proc:2007016.
[45] M. Breuer, N. Peller, Ch. Rapp, and M. Manhart. Flow over periodic hills: Numerical and experimental study in a wide range of Reynolds numbers. *Computers & Fluids*, 38(2):433–457, 2009.
[46] J. Frohlich, C.P. Mellen, W. Rodi, L. Temmerman, and M.A. Leschziner. Highly resolved large-eddy simulation of separated flow in a channel with streamwise periodic constrictions. *Journal of Fluid Mechanics*, 526:19–66, 2005.
[47] P. R. Spalart. Young person's guide to detached-eddy simulation grids. Technical Report CR-2001-211032, NASA, 2001.

https://doi.org/10.4208/cicp.220715.150416a Published online by Cambridge University Press